Int. J. Multiphase Flow Vol. 18, No. 6, pp. 831–845, 1992
Printed in Great Britain.

0301-9322/92 $5.00 + 0.00

SPATIAL DISTRIBUTION OF VOID FRACTION WITHIN A LIQUID SLUG AND SOME OTHER RELATED SLUG PARAMETERS

R. VAN HOUT, L. SHEMER and D. BARNEA
Department of Fluid Mechanics, Faculty of Engineering, Tel-Aviv University, Ramat-Aviv 69978, Israel

(Received 16 March 1992; in revised form 7 July 1992)

Abstract—The structure of vertical upward slug flow in a pipe is studied. The distribution of the phases in the Taylor bubble zone and the liquid slug zone is investigated by simultaneous measurements with two optical fiber probes. In the Taylor bubble zone the shape of the Taylor bubble and the distribution of the bubble length is reported. In the liquid slug region, the distribution of the void fraction is obtained over a dense grid in both the axial and radial directions. These experimental results shed some light on the hydrodynamics of the two-phase slug flow, in particular regarding the production of the dispersed bubbles and their distribution along the liquid slug.

Key Words: slug flour, void fraction

1. INTRODUCTION

Gas–liquid flow in pipes may appear in various configurations determined by the spatial distribution of the two phases in the pipe. These configurations are termed as flow patterns. One of the most complex flow patterns with unsteady intermittent characteristics is the slug flow. Slug flow exists over a broad range of gas and liquid flow rates and is encountered in a wide variety of industrial applications.

In vertical slug flow, most of the gas is located in large bullet-shaped bubbles, the so-called Taylor bubbles, which occupy most of the pipe cross section. The liquid confined between the Taylor bubble and the pipe wall flows around the Taylor bubble as a thin film. The Taylor bubbles are separated by liquid slugs which may contain small bubbles.

Due to the complex nature of slug flow, rigorous continuum equations for slug flow cannot be formulated. However, a variety of approximate models have been developed which allow calculation of the slug hydrodynamic parameters. The first comprehensive models for slug flow were introduced by Dukler and his coworkers, i.e. by Dukler & Hubbard (1975) for horizontal flow and by Fernandes *et al.* (1983) for vertical flow. Various options for modeling the hydrodynamic parameters and pressure drop have been proposed recently by Taitel & Barnea (1990). They used a unified approach that is applicable for vertical and horizontal, as well as inclined, cases. The physical models that have been suggested require input information about the following parameters: the translational velocity, U_T; the dispersed bubble velocity, U_B; the liquid holdup in the liquid slug, R_s; and the liquid slug length, l_s. These quantities may be obtained either experimentally or by applying some physical models. A comprehensive presentation related to the aforementioned parameters is outlined in Fabre & Line (1992).

Most of the data regarding R_s is related to the volume average R_s in the liquid slug. Gregory *et al.* (1978) measured the liquid volume fraction in horizontal slugs by a capacitance-type sensor. Heywood & Richardson (1979) used the γ-ray absorption method to determine the average holdup in horizontal liquid slugs. Schmidt (1977) measured the liquid holdup in the liquid slug in vertical risers using a capacitance sensor. Fernandes (1981) measured R_s in vertical air–water slug flow in a 0.05 m i.d. pipe by "quick-closing valves". Barnea & Brauner (1985) proposed a method for estimating the gas holdup within the liquid slug which applies to vertical horizontal and inclined flows. The calculated values of R_s range from 1 to 0.48, with the value of 0.48 being associated with the maximum volumetric packing of the dispersed bubbles in the liquid slug. For the particular case of vertical and off-vertical pipes of relatively large diameters [$D > 0.05$ m for air–water flows (Taitel *et al.* 1980)], the maximum value of R_s is about 0.75, as reported by Fernandes (1981).

Barnea & Shemer (1989) used a conductance probe to detect the passage of the gas–liquid interface at the centerline of a vertical tube with 0.05 m i.d. in upward air–water slug flow. The recorded information was further processed to obtain the liquid slug holdup at various axial locations along the liquid slug, as well as the slug length. The experimental values of the liquid holdup range from $R_s = 0.75$ on the transition to bubbly flow, to $R_s = 0.4$ near the transition to churn flow.

Mao & Dukler (1989) measured the local holdup in the liquid slug using a radio frequency local probe. The radial distribution of the void fraction was reported in this study for a single pair of liquid and gas flow rates. The axial voidage variation along the liquid slug was quite similar for all radial locations considered.

The mechanism responsible for the presence of small dispersed bubbles in the liquid slug is not yet fully understood. It is usually acceptable that gas is exchanged between the elongated bubble and the liquid slug (Fernandes *et al.* 1983; Andreussi & Bendiksen 1989). Small bubbles are produced due to the tearing from the Taylor bubble tail and dispersed into the liquid slug. The dispersed bubbles are then recaptured by the next elongated bubble which comes along.

In the present work, fiber optics tip probe measurements were performed over a dense two-dimensional grid in order to gain information about the detailed spatial structure of the voidage distribution in the liquid slug. This information allows one to draw certain conclusions regarding the hydrodynamics of the gas–liquid slug flow and to understand better the mechanisms which are responsible for the bubble generation and distribution within the slug. The experiments performed in the course of the present study allow some additional important slug parameters to be extracted, such as the slug and Taylor bubble length distributions, the shape of the Taylor bubble etc.

2. EXPERIMENTAL SYSTEM AND DATA ACQUISITION

The experimental system consists of a 10 m vertical perspex pipe with 0.05 m i.d. Air is supplied from a central high-pressure line, the pressure reducer maintains a constant gauge pressure of 1 bar. Liquid is supplied from a 1500-litre tank and is circulated in a closed loop. The inlet device is of a "mixer"-type. The air is introduced circumferentially into the pipe through uniformly distributed small holes with dia 1 mm. The length of the air inlet device is about 0.3 m. The water enters the inlet in the axial direction through a pipe with the same diameter as the test section.

The local void fraction measurements were carried out with optical fiber sensors which have high frequency response and good spatial resolution due to a very small fiber tip diameter (of the order of a few μm) which does not disturb the flow. The measurement is based on the reflection variation at the probe tip due to the difference in the refraction coefficients of air and water. The passage of an air bubble at the fiber tip is detected easily, due to a sudden increase in the intensity of the reflected light.

Two optical fiber sensors were used simultaneously. They were installed at the same axial position in the pipe at about 6 m from the inlet device. One of the optical fiber sensors was placed stationary at the centerline of the pipe. The second sensor was installed in such a way that its radial position in the pipe could be changed easily. This was accomplished by a traversing mechanism mounted on the pipe. The center probe serves as a reference which enables the determination of the locations of the interface between the Taylor bubbles and liquid slugs, and ensures constant experimental conditions at various radial positions.

Measurements were taken at 11 radial positions in the pipe, including the centerline, namely at distances of $y = 1, 2, 3, 4, 5, 6, 7, 10, 15, 20$ and 25 mm relative to the pipe wall. The measurements were carried out for the 8 flow conditions shown in table 1.

The signals from the two optical fiber sensors are processed to yield the corresponding TTL outputs with two voltage levels representing the instantaneous phase (gas or liquid) at each fiber tip. The output signals from both sensors are sampled continuously by a computer using a 12-bit A/D converter with a sampling frequency of 10 kHz/channel. The total duration of the continuous sampling for any given experimental condition varied from 10 to about 30 min, depending on the flow condition. All sampled information was recorded on a magnetic tape for further processing.

Table 1. Experimental flow conditions

Flow condition	U_{LS}(m/s)	U_{GS}(m/s)	Flow pattern
1	0.01	0.10	Bubble flow
2	0.01	0.25	Slug flow
3	0.01	0.63	Slug flow
4	0.01	1.56	Slug–churn flow
5	0.10	0.41	Slug flow
6	0.10	0.63	Slug flow
7	0.25	0.41	Slug flow
8	0.75	0.75	Slug flow

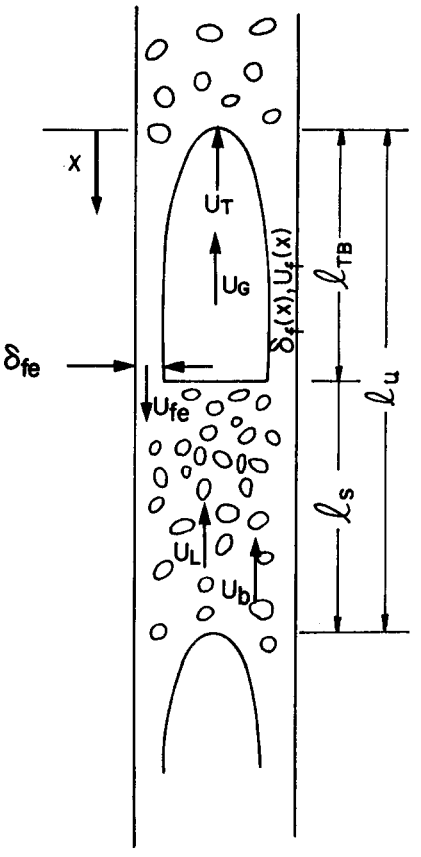

Figure 1. The geometry of vertical upward slug flow.

The recorded binary signals from both sensors were processed to extract the following information:

- The spatial distribution of the void fraction within the liquid slug.
- The mean liquid slug length and the liquid slug length distribution.
- The mean Taylor bubble length and the Taylor bubble length distribution.
- The Taylor bubble shape.

More details about the experimental facility, as well as on data acquisition and processing, are given in van Hout (1991).

3. EXPERIMENTAL RESULTS AND DISCUSSION

For the sake of convenience, the slug flow variables are now introduced using a sketch of slug flow as shown in figure 1. The slug unit of length l_u is usually subdivided into two main sections: the liquid slug zone of length l_s; and the Taylor bubble zone, or the film zone, of length l_{TB}. The liquid slug contains small dispersed bubbles with a bulk void concentration of $\epsilon_s = 1 - R_s$, R_s being the liquid holdup. The average liquid velocity in the liquid slug is designated U_L, and the average axial velocity of the dispersed bubbles in the liquid slug is denoted U_b.

The Taylor bubble zone consists of an elongated gas bubble and a liquid film. The translational velocity of the Taylor bubble, U_T, is the velocity at which the Taylor bubble propagates downstream. If one moves at the velocity U_T, the slug unit is seen as frozen. The average velocity in the liquid film is designated U_f, while that of the gas in the Taylor bubble is designated U_G. The film thickness is δ_f and the liquid film holdup $R_f = A_f/A$. Note that $U_f = U_f(x)$ and $R_f = R_f(x)$ are functions of the distance x from the bubble's top (or slug "tail"). A complete axial symmetry is assumed in the present work.

The first step in the analysis of the data is to distinguish between the liquid slug and the Taylor bubble regions. This distinction is based on measurements by the centerline probe. In this study only the bubbles longer than the pipe diameter D are considered to be Taylor bubbles (cf. Barnea & Shemer 1989). This corresponds to a bubble duration of D/U_T. Since two successive Taylor bubbles which are separated by a very short liquid slug coalesce and create a larger Taylor bubble, a minimum liquid slug length of twice the pipe diameter is assumed. In this case, the consecutive Taylor bubbles separated by a short liquid bridge are seen by the processing procedure as a single bubble.

3.1. Liquid Slug Length Distributions

About 2000–2500 slug units were detected and analyzed for each flow condition given in table 1. Some representative distributions of the liquid slug length are depicted in figure 2. At all the flow conditions in table 1, except those presented at figure 2(C), the mean liquid slug length varies from $15D$ to $19D$ with a standard deviation of about 30%. At high mixture velocity the histogram is somewhat flatter, with a standard deviation of about 40% [figure 2(D)]. Slug length distribution histograms with a well-defined peak around $l_s = 16D$ indicate that the slug flow under consideration is stable and well-developed. Contrary to this, figure 2(C) represents flow conditions corresponding to undeveloped slugs, where the relative contribution of very short slugs is considerable, so that the mean slug length is about $8D$. At this high gas flow rate, the flow pattern is close to the transition to churn flow.

It is well-known that the stable slug length is relatively insensitive to the gas and liquid flow rates and is fairly constant for a given pipe diameter. The stable liquid slug length is reported to be between $10D$ to $20D$ (Moissis & Griffith 1962; Akagawa & Sakaguchi 1966; Fernandes 1981; Barnea & Shemer 1989). A theoretical reasoning for these values of the stable slug length can be found in Taitel *et al.* (1980), Dukler *et al.* (1985) and Shemer & Barnea (1987). Although these models are based on different concepts, all of them suggest that the minimum stable slug length is related to the distance needed to reestablish a fully developed velocity distribution in the liquid slug.

3.2. Taylor Bubbles—Length and Shape

The length of the Taylor bubble, l_{TB}, its shape, $\delta_f(x)$ (or $R_f(x)$), the velocity profile along the liquid film, $U_f(x)$, and especially the values of the film thickness and its velocity just before pickup,

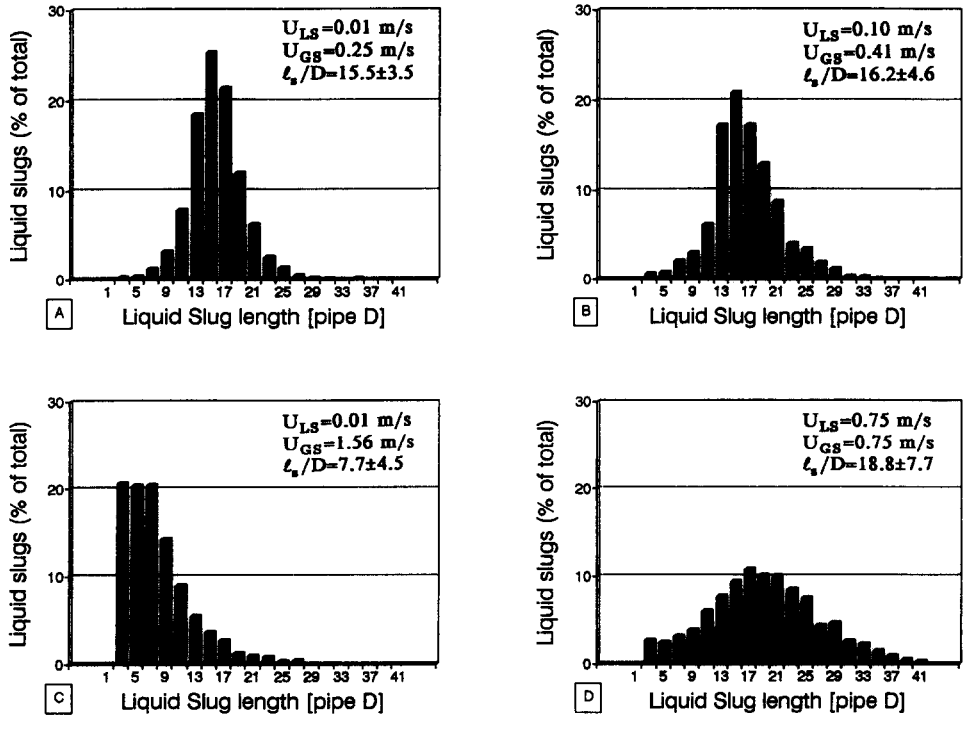

Figure 2. Liquid slug length distribution.

δ_{fe} and U_{fe}, are important parameters for calculating the pressure drop and heat at mass transfer in slug flow.

The actual shape of the Taylor bubble (or the liquid film) is very complex, especially near the Taylor bubble "nose". A reasonable approximation to the reality is to use the one-dimensional approach usually adopted in open channel flow theory. This method has been used by Dukler & Hubbard (1975) and Nicholson *et al.* (1978) for horizontal flow and by Taitel & Barnea (1990) for the inclined and vertical cases. Barnea (1990) showed the importance of considering the bubble shape in order to calculate accurately the pressure drop in slug flow.

Assuming incompressible flow (within any considered slug unit), a momentum balance on the liquid film relative to a coordinate system moving with a velocity U_T yields the following differential equation for U_f (cf. Barnea 1990):

$$\frac{dU_f}{dx} = -\frac{g\left(1-\frac{\rho_G}{\rho_L}\right)}{U_T - U_f} + \frac{\frac{2}{D}f_w}{(U_T - U_L)R_s} U_f|U_f|. \quad [1]$$

This equation is based on the assumption that the gas–liquid interfacial shear stress and the pressure drop along the Taylor bubble are negligible.

Equation [1] is solved numerically for the film velocity $U_f(x)$. The corresponding holdup of the liquid film R_f, i.e. the Taylor bubble shape, is found by using the mass balance equation

$$R_f(U_T - U_f) = R_s(U_T - U_L). \quad [2]$$

The integration of [1] is performed until the gas mass balance over a slug unit is satisfied:

$$U_{GS} = U_b(1 - R_s) + U_T R_s \frac{l_{TB}}{l_u} - \frac{U_T}{l_u}\int_0^{l_{TB}} R_f \, dx. \quad [3]$$

The evaluation of all the terms in [1]–[3] is discussed in detail in Barnea (1990). This procedure yields the length of the Taylor bubble l_{TB}, as well as the holdup R_{fe} and the film velocity U_{fe} at the end of the liquid film just before pickup. In the present work, two solutions for the Taylor bubble shape are considered. In the first case, [1] was applied to the whole length of the Taylor bubble, from the tail of the leading slug to the rear of the following slug. The liquid film region is assumed to be free of entrained bubbles. In order to assure continuity between the liquid slug zone and the film zone, the following boundary condition is adopted: at the top of the Taylor bubble ($x = 0$), $U_f = U_L$ and $R_f = R_s$.

In the second case, the Taylor bubble nose is assumed to be spherically shaped with a diameter of $D_c = 0.75D$, as suggested by Dumitresku (1943). Contrary to the previous case, where all dispersed bubbles were entrained into the Taylor bubble at the top $x = 0$, in this approximation the film zone along the spherical portion of the Taylor bubble cap is not free of dispersed bubbles and their concentration changes gradually, so that at the end of this portion the film is free of entrained bubbles. The liquid holdup along the liquid film zone of the spherical cap region $R_{fc}(x)$ is assumed to decrease linearly:

$$R_{fc}(x) = (R_{fce} - R_s)\frac{x}{D_c} + R_s, \quad [4]$$

where

$$R_{fce} = 1 - \frac{D_c^2}{D^2}. \quad [5]$$

From the end of the spherical portion of the bubble cap, the momentum equation [1] is applied, with the initial conditions $U_f = U_{fce}$ and $R_f = R_{fce}$ at $x = D_c$.

The simultaneous void measurements by two tip probes, one located at the centerline and the second at variable radial locations, allowed the measurement of the Taylor bubble length and shape. The Taylor bubble length distribution is presented in figure 3 for a number of flow conditions. For a given liquid flow rate, both the mean Taylor bubble length, $\langle l_{TB} \rangle$, and the standard deviation, σ_{TB}, increase with increasing gas superficial velocity and the Taylor bubble length distribution becomes considerably more uniform. More examples are given in van Hout

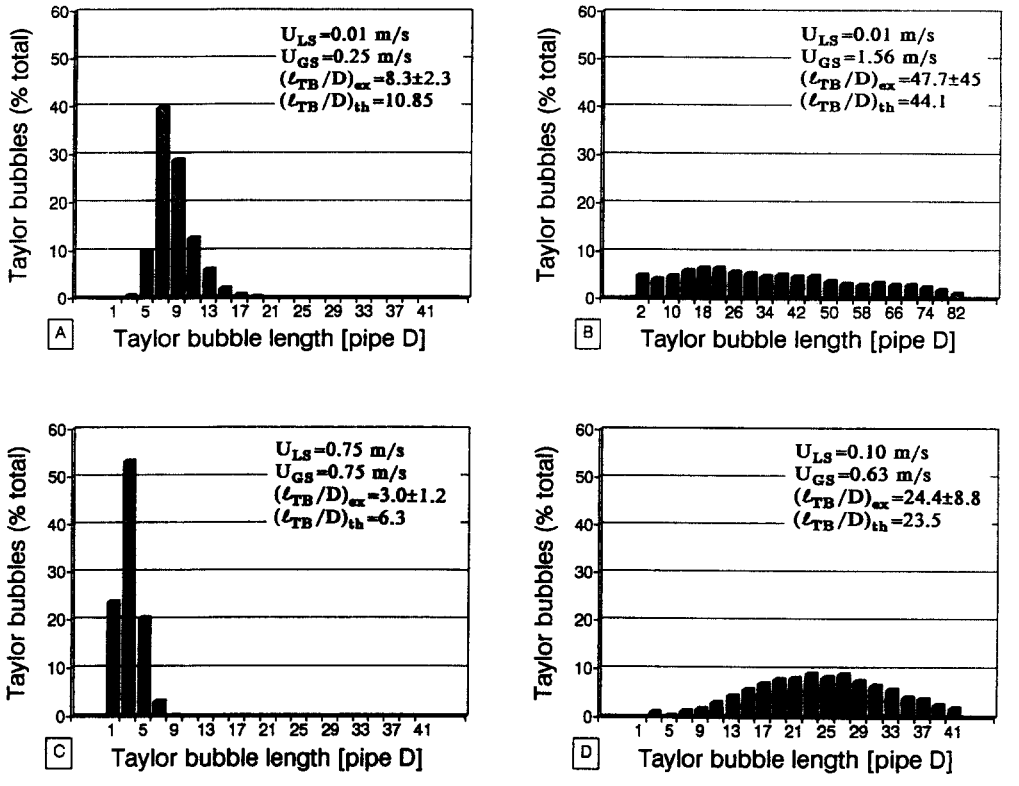

Figure 3. Taylor bubble length distribution.

(1991). Note that the histogram in figure 3(B), which corresponds to flow conditions close to those of churn flow, is particularly flat. The distinction between the Taylor bubbles and the dispersed bubbles is not clear-cut in this case (cf. Barnea & Shemer 1989).

The measured mean Taylor bubble length was compared with the theoretical prediction of the model presented above (see figure 3). Note that both cases considered in the model yield essentially the same Taylor bubble length. Under all the experimental conditions in table 1, the experimental and predicted results are in quite good agreement for Taylor bubbles which are sufficiently long, $l_{TB} > 10D$ (relative discrepancy being up to 10%). For very short Taylor bubbles, however, the discrepancy is considerable [figure 3(C)], with the theoretical estimate being substantially higher than the experimental data. Note that for short Taylor bubbles, the bubble nose (the portion until the liquid film attains its terminal constant thickness) constitutes a considerable part of the total Taylor bubble length. This, on the one hand, leads to greater sensitivity of the theoretical results to the model assumptions in the nose region, and on the other hand, the intrinsic oscillations of the bubble nose in the experiments result in underestimation of the actual bubble length.

The comparison between the experimental and theoretical bubble shape is shown in figure 4. The bubble shape in the nose region is not very sensitive to flow conditions. Note that both theoretical cases considered in the model resulted in a similar shape of the bubble profile. The experimental bubble cap shows a more moderate curvature than the theoretical one. Similar results regarding the theoretical bubble shape, as well as the discrepancy between the experiments and the theory, were obtained by Mao & Dukler (1991), who employed a more rigorous theoretical approach.

3.3. *Void Fraction in the Liquid Slug*

The two-dimensional voidage distribution $\epsilon(x, y)$ within the liquid slug has been investigated, the radial coordinate $y = R - r$ being the distance from the wall, whereas the axial coordinate x represents the distance relative to the bottom of the Taylor bubble. At each radial location, the sampled data were averaged over a relatively short time "window", which corresponds to the passage of a column of the length of 1 pipe diameter, D, at the translational velocity of the Taylor

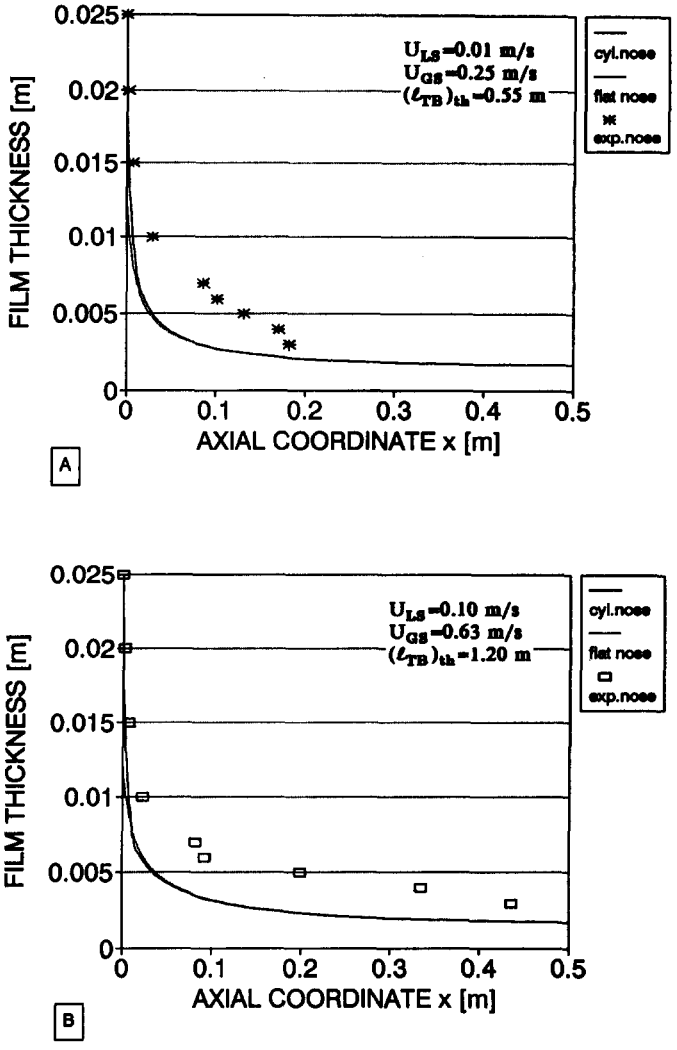

Figure 4. Taylor bubble shape.

bubble. The first window starts at the top of the liquid slug, as defined by the central probe. In the case of a non-flat bottom of the Taylor bubble, the first window length at off-axis locations may be somewhat different from D. The considered liquid slug is "filled up" with full windows, each new window starting at the end of the former one. Thus, each window number corresponds to a certain axial position in the liquid slug and the axial position in the middle of the window is given by $x = (i - 1/2)D$, where i is the window number in the liquid slug.

Short-time averaging of the void fraction was performed over each window separately. The number of sampled data points averaged in each window at any given radial location was of $O(10^3)$. This procedure was employed for each slug unit. Finally, the local void fraction was obtained by applying the ensemble-averaging procedure (Van Atta 1974) over all slug units sampled at any given flow condition. Each value of $\epsilon(x, y)$ therefore represents averaging of $O(10^6)$ data points.

To sum up, the local void fraction $\epsilon(x, y)$ is calculated on a two-dimensional grid within the liquid slug, where the radial grid coordinate, y corresponds to the probe distance from the wall, while the axial coordinates are spaced by distances equal to the pipe diameter.

3.3.1. Distribution of the local voidage in the liquid slug

The local void fraction $\epsilon(x, y)$ at various flow conditions can be presented as a surface in three-dimensional space. Details of these distributions can be seen in a more convenient way in the cross sections of the three-dimensional figures in either the radial or axial directions. Figure 5

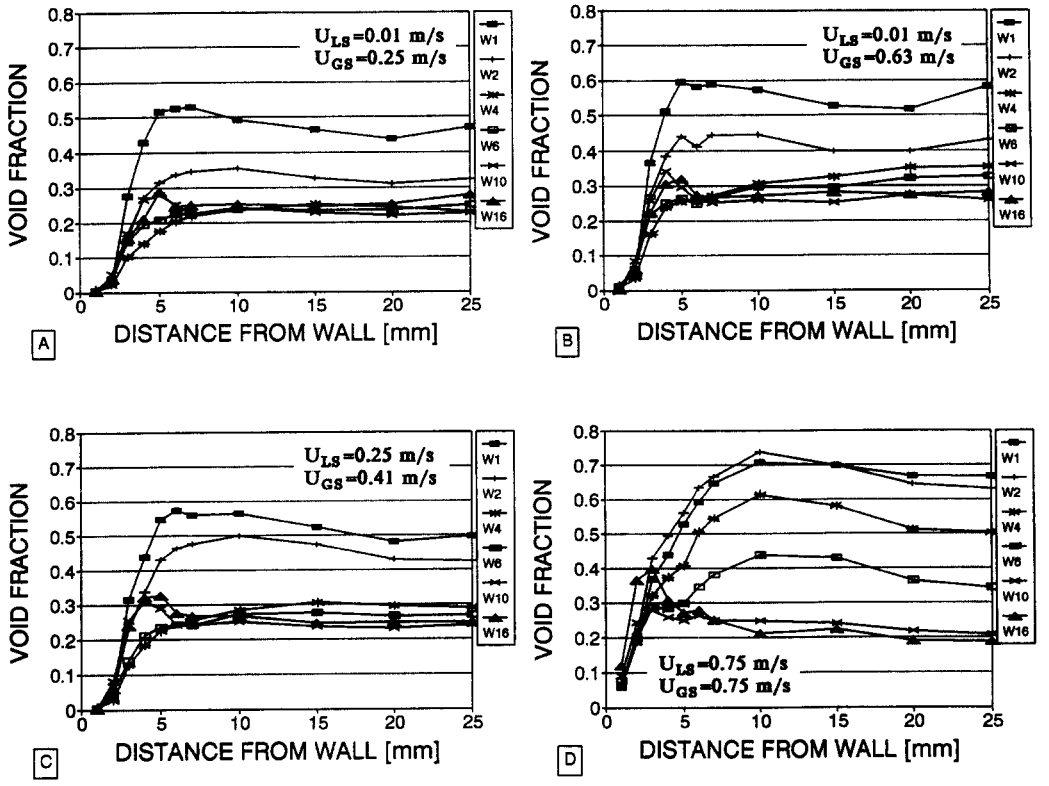

Figure 5. Radial void fraction distribution at various axial positions.

shows some typical examples of the development of the radial voidage distribution at several axial locations corresponding to windows 1, 2, 4, 6, 10 and 16. The evolution of the voidage distribution along the liquid slug is quite similar for all flow conditions studied. In all cases, the immediate vicinity of the wall (until $y \simeq 2$ mm) is almost free of gas bubbles with negligible voidage. In the first window, the void fraction is substantially higher than in the following windows. The void fraction increases sharply from nearly zero at $y = 2$ mm to a maximum at about $y = 5$ to 7 mm. Then the radial void fraction decreases to a moderate minimum and increases again towards the centerline of the pipe. In the second window, the radial voidage distribution remains similar to that of the first window, with slightly lower values of the void fraction throughout the whole cross section. In windows 4 and 6, the general shape of the radial void fraction distribution becomes quite different, and the value of the void fraction throughout the whole pipe cross section is substantially lower than that close to the Taylor bubble. The void fraction increases monotonously until $y \simeq 5$ to 7 mm, and then remains nearly constant until the center of the pipe. Further away from the Taylor bubble, at windows 10 and 16, the shape of the voidage profile changes again. A voidage peak is observed at $y \simeq 4$ mm, the value of ϵ then decreases slightly and levels off until the center of the pipe. Note that at $y \simeq 4$ mm the void fraction far from the Taylor bubble exceeds the void fraction values at windows 4 and 6.

These voidage profiles suggest that the liquid slug can be divided into three distinct regions. The first region, which is of the length of about 2 or 3 pipe diameters in the immediate vicinity behind the Taylor bubble, is referred to as a wake region. The region from about $x = 10D$, where the voidage radial profiles attain its permanent shape, is the developed region of the liquid slug, while the region between can be considered as an intermediate region. The radial distributions in the developed region of the liquid slug are similar to those in dispersed bubble flow pattern, where a voidage peak near the wall appears, as has been observed by Serizawa *et al.* (1975), Herringe & Davis (1976), Zun (1988) and Zun & Moze (1990).

A different insight into the local voidage distribution can be obtained by examining the axial variation of the voidage along the liquid slug at different radial locations. Typical patterns of such axial distributions are shown in figure 6(A). The patterns at other flow conditions are of a similar

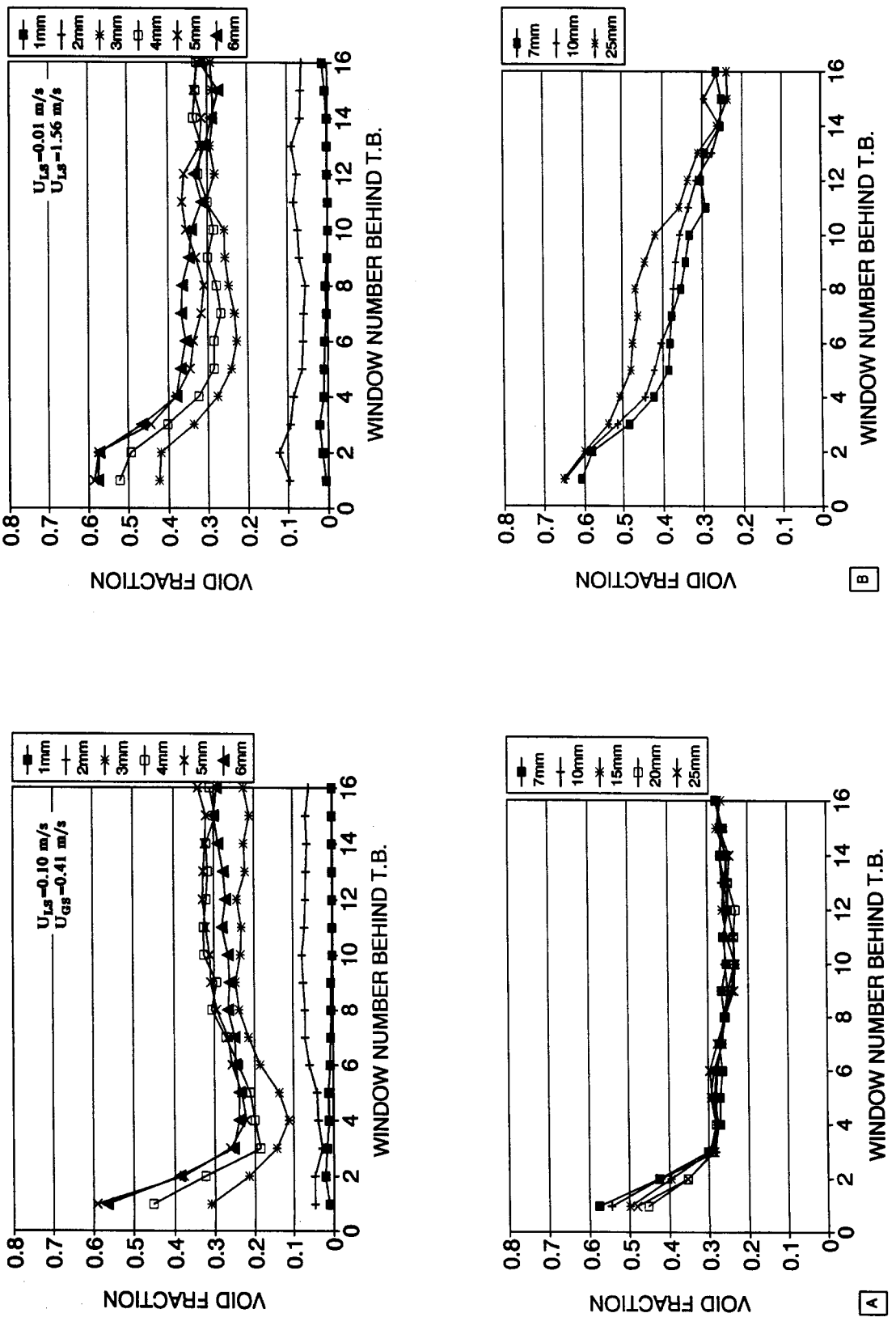

Figure 6. Axial void fraction distribution at various radial positions.

nature and are given in van Hout (1991). Three different shapes of the axial distribution of the void fraction can be identified. Close to the wall, the void fraction remains low throughout the whole slug length. In the central portion of the pipe ($y > 7$ mm), the axial voidage distribution is of the same nature for all radial positions. The void fraction exhibits a steep decrease from a high value in the wake region until about $x = 3D$, and then remains almost constant along the rest of the slug. In the range $3 < y < 7$ mm, the axial distribution of ϵ has a different shape with a well-defined minimum at the end of the wake region. At high flow rates, the overall pattern is somewhat different [figure 6(B)]. The same three shapes of distribution can still be defined, but the

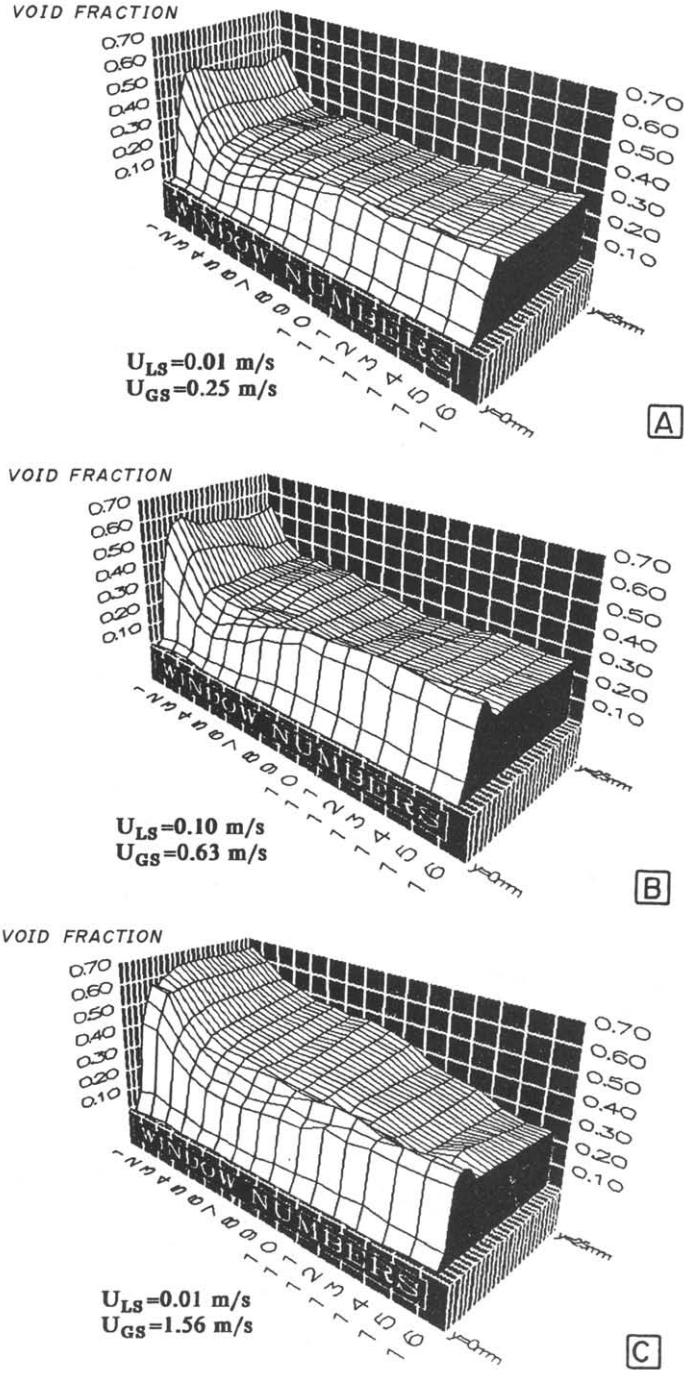

Figure 7. The two-dimensional void fraction distribution within the liquid slug.

slug does not attain a fully developed stage, the wake is notably longer and the rest of the slug is an undeveloped transitional region.

The three-dimensional surface of the void fraction in the liquid slug is depicted in figure 7. In these figures the "wake region", the "translational region" and the "developed region" can be clearly seen. The extension of the wake region increases with the mixture velocity. The flow pattern in figure 7(C) is close to the transition from slug to churn flow. The fact that the slug remains undeveloped even at $x = 16D$ is clearly seen.

The measured radial and axial void fraction distributions suggest the following picture of the dispersed bubble dynamics in the liquid slug. The streamline structure behind the Taylor bubble is shown schematically in figure 8. When the liquid film penetrates into the liquid slug, it behaves similarly to a wall jet (Shemer & Barnea 1987). The liquid streamlines (relative to a coordinate system moving with the translational velocity U_T) expand towards the centerline and the region just behind the Taylor bubble forms a "closed" wake in which the liquid circulates, as shown in figure 8. At the rear of the Taylor bubble this annular wall jet tears bubbles from the outer periphery of the Taylor bubble due to the high shear at the film–gas interface. These bubbles follow approximately the streamlines of the eddies within the wake. Out of the confined wake, bubbles are continuously swept into the liquid slug body, primarily at the bottom of the wake, which acts as a bubble injector. Bubbles are released from the wake around the centerline and penetrate into the slug body spreading throughout the whole pipe cross section, thus creating a spatial voidage distribution of a "bottleneck" shape.

This qualitative suggested picture is based on the observed voidage distributions in the axial and radial directions in the wake and the transitional region. A schematic presentation of the bubble distribution is superimposed on the streamline pattern in figure 8. In the wake region the absolute values of void fraction are high due to high turbulence in this region. The movement of the bubbles

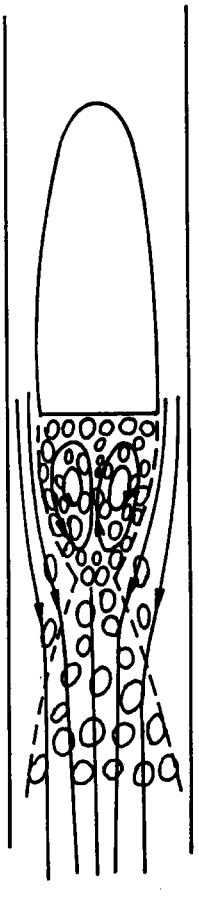

Figure 8. The liquid streamline structure and the dispersed bubble distribution in the liquid slug.

in the wake along the eddies results in a peak in void fraction near the circumference and at the center of the wake, while the core of the wake shows a slight minimum (cf. figure 5). In the transitional region, at the bottom of the wake ($x \simeq 3D$), the void fraction is maximum at the center. The "bottleneck" shape of the voidage distribution at the bottom of the wake may indicate that bubbles are released from the wake region mainly near the centerline, thus resulting in a decreasing voidage while approaching the wall [cf. figure 6(A) for $3 < y < 6$ mm, as well as figure 5—windows 4 and 6]. This description is in agreement with the flow visualization of Campos & Guedes De Carvalho (1988a). They photographed the wakes of a single Taylor bubble penetrating a dye–clear water interface and observed a similar "bottleneck" shape. They also obtained experimentally a wake length of about $3D$ (Campos & Guedes De Carvalho 1988b).

The radial voidage distribution in the developed region of the liquid slug shows a voidage peak near the wall at all flow conditions employed in this study. Similarly shaped voidage distributions have been observed in bubbly flow (Serizawa *et al.* 1975; Zun & Moze 1990).

3.3.2. Spatially averaged void fraction distributions in the liquid slug

The local measured void fraction $\epsilon(x, y)$ can be used to obtain the averaged void fraction over the pipe cross section at different axial locations along the slug. Alternatively, the local void fraction can be averaged along the liquid slug at various radial positions. Averaging in both directions yields the overall mean void fraction in the liquid slug.

The averaged cross-sectional void fraction along the liquid slug $\epsilon_y(x)$ is shown in figure 9 for a number of flow conditions. For all measured cases, the average cross-sectional void fraction in the wake region is considerably higher than in the developed region. The general shape of the integrated profiles resembles that of the local void fraction distribution in the liquid slug in the central portion of the pipe [cf. figures 6(A) and 6(B)]. In all cases, the average void fraction attained nearly the same value of about 0.22 in the fully developed zone of the liquid slug. The results of figure 9 show that the extent of the wake region increases with increasing mixture velocity. It is interesting to note, however, that although the mixture velocities in figures 9(C) and 9(D) are almost

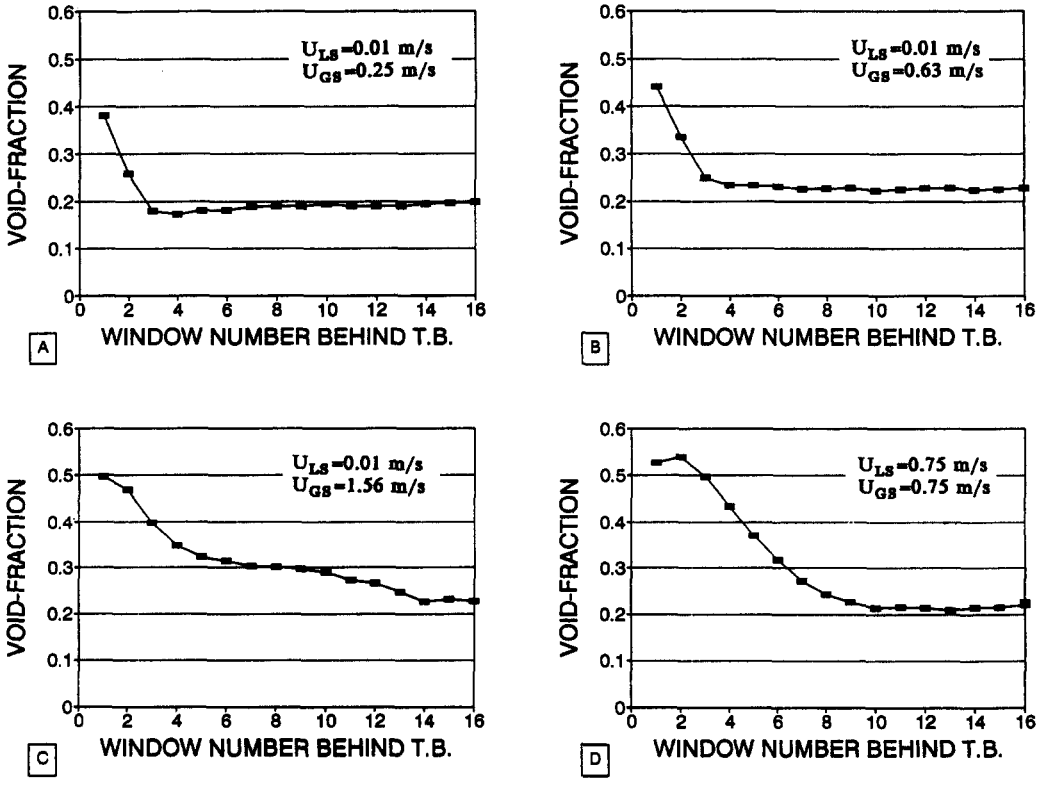

Figure 9. Average cross-sectional void fraction $\epsilon_y(x)$ at various axial positions.

the same, the wake region is substantially longer at the higher gas superficial velocity [figure 9(C)]. This can be explained by the fact that the extent of the wake is determined not only by the mixture velocity, but also by the rate of shear of the annular jet at the bottom of the Taylor bubble. The Taylor bubbles are considerably longer in figure 9(C) as compared to figure 9(D) (cf. figure 3). The liquid film velocity increases with increasing length of the Taylor bubble [until the terminal liquid film velocity is attained (Barnea 1990)], causing a much higher shear velocity in the case presented in figure 9(C).

Some examples of the mean void fraction averaged over the total length of the liquid slug at various radial positions $\epsilon_x(y)$ are shown in figure 10. All the radial distributions $\epsilon_x(y)$ look quite similar, in spite of the fact that the local radial distributions of the voidage are different, in particular in the wake region (cf. figure 5). This indicates that the contribution of the voidage in the wake region to the average voidage along the liquid slug is relatively small.

The overall mean void fraction in the liquid slug $\epsilon_{x,y}$ as a function of the mixture velocity, U_M, is given in figure 11 and is compared with the available data of Mao & Dukler (1989), Fernandes (1981) and Barnea & Shemer (1989). These data also provide voidage results in bubble and churn flow. Note that the results of Mao & Dukler (1989) and Barnea & Shemer (1989) represent the averaged voidage in the liquid slug measured at the centerline, while the results of Fernandes (1981) and those of this study represent the volumetric-averaged void fraction in the liquid slug.

A model to predict the average voidage within the liquid slug was suggested by Barnea & Brauner (1985). The predicted results are shown in figure 11 for comparison. The model suggests that the gas holdup at the transition line from dispersed bubbles is the maximum holdup that the liquid slug can accommodate as a fully developed bubbly flow at a given mixture velocity U_M. Thus, curves of constant U_M represent the locus where $\epsilon_{x,y}$ is constant and is equal to the holdup of the dispersed bubble pattern at the transition boundary. Once the fluid properties and the pipe geometry are set, $\epsilon_{x,y}$ can be obtained from the theoretical transition boundary to dispersed bubble flow, as suggested by Barnea (1987).

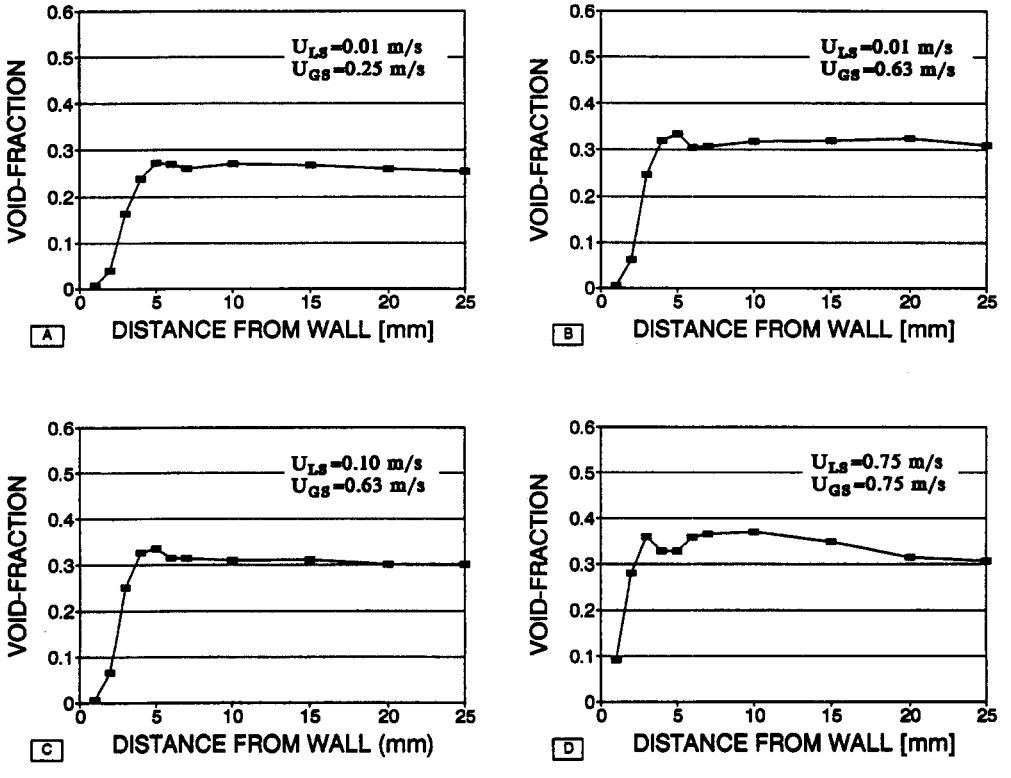

Figure 10. Mean void fraction averaged over the total length of the liquid slug $\epsilon_x(y)$ at various radial positions.

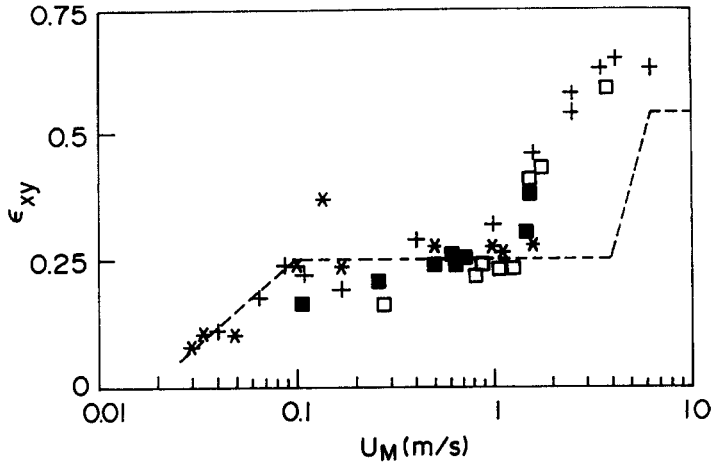

Figure 11. Overall mean void fraction in the liquid slug $\epsilon_{x,y}$ as a function of the mixture velocity: ■, present results; +, Barnea & Shemer (1989); *, Fernandes (1981); □, Mao & Dukler (1989); ---, Barnea & Brauner (1985).

The measured mean void fraction $\epsilon_{x,y}$ compares quite well with the predicted results. The predictive model, however, deviates from the experimental data at relatively high mixture velocities. This discrepancy can result from the fact that the model suggested by Barnea & Brauner (1985) assumed developed liquid slugs, while for very high mixture velocities, the relative number of very short undeveloped liquid slugs may become high, as shown in the histogram in figure 2(C). Under these conditions, the significant contribution of the wake region results in substantially higher values of the overall mean void fraction.

4. SUMMARY AND CONCLUSIONS

Detailed measurements of the local void fraction performed simultaneously by two fiber optics probes provide information on the gas distribution along the slug unit. These measurements enabled us to obtain the two-dimensional spatial distribution of the void fraction in the frame of reference relative to the moving Taylor bubble. In the Taylor bubble zone, both the shape and length distributions of the elongated bubbles were measured. In the liquid slug zone, the slug length and voidage distributions were determined. In this zone the local void fraction measurements were performed over a dense grid. The spatial voidage distribution obtained in the liquid slug zone is related to the streamline pattern behind the Taylor bubble.

Three distinct regions can be defined in the liquid slug with respect to the voidage distribution. Closest to the Taylor bubble is the wake region in which the voidage is a maximum and the bubbles torn from the Taylor bubble follow the wake region vortices. The extent of the wake region is about a few pipe diameters and increases with increasing mixture velocity. Far away from the Taylor bubble, at distances exceeding about $10D$, the radial voidage distribution no longer changes notably and the voidage is substantially lower than in the wake region. In this developed region of the liquid slug the radial voidage distribution strongly resembles that observed in dispersed bubble flows. The intermediate region is defined as the transition between the wake and the developed slug region. The bubbles are injected into this intermediate region from the bottom of the wake mainly near the pipe axis and are gradually spread across the whole pipe.

REFERENCES

AKAGAWA, K. & SAKAGUCHI, T. 1966 Fluctuation of void ratio in two-phase flow (2nd report, Analysis of flow configuration considering the existence of small bubbles in liquid slugs). *Bull. JSME* **9**, 104–110.

ANDREUSSI, P. & BENDIKSEN, K. 1989 An investigation of void fraction in liquid slugs for horizontal and inclined gas–liquid pipe flow. *Int. J. Multiphase Flow* **15**, 937–946.

BARNEA, D. 1987 A unified model for predicting flow-pattern transitions for the whole range of pipe inclinations. *Int. J. Multiphase Flow* **13,** 1–12.

BARNEA, D. 1990 Effect of bubble shape on pressure drop calculations in vertical slug flow. *Int. J. Multiphase Flow* **16,** 79–89.

BARNEA, D. & BRAUNER, N. 1985 Holdup of the liquid slug in two-phase intermittent flow. *Int. J. Multiphase Flow* **11,** 43–49.

BARNEA, D. & SHEMER, L. 1989 Void-fraction measurements in vertical slug flow: applications to slug characteristics and transition. *Int. J. Multiphase Flow* **15,** 495–504.

CAMPOS, J. B. L. M. & GUEDES DE CARVALHO, J. R. F. 1988a An experimental study of the wake of gas slugs rising in liquids. *J. Fluid Mech.* **196,** 27–37.

CAMPOS, J. B. L. M. & GUEDES DE CARVALHO, J. R. F. 1988b Mixing induced by air slugs rising in narrow columns of water. *Chem. Engng Sci.* **43,** 1569–1582.

DUKLER, A. E. & HUBBARD, M. G. 1975 A model for gas–liquid slug flow in horizontal and near horizontal tubes. *Ind. Engng Chem. Fundam.* **14,** 337–347.

DUKLER, A. E., MARON, D. M. & BRAUNER, N. 1985 A physical model for predicting the minimum stable slug length. *Chem. Engng Sci.* **40,** 1379–1386.

DUMITRESCU, D. T. 1943 Strömung an einer Luftblase im senkrechten Rohr. *Z. Angew. Math. Mech.* **23,** 139–149.

FABRE, J. & LINE, A. 1992 Modeling of two-phase slug flow. *A. Rev. Fluid Mech.* **24,** 21–46.

FERNANDES, R. C. 1981 Experimental and theoretical studies of isothermal upward gas–liquid flows in vertical tubes. Ph.D. Dissertation, Univ. of Houston, TX.

FERNANDES, R. C., SEMIAT, R. & DUKLER, A. E. 1983 Hydrodynamic model for gas–liquid slug flow in vertical tubes. *AIChE Jl* **29,** 981–989.

GREGORY, G. A., NICHOLSON, M. K. & AZIZ, K. 1978 Correlation of the liquid volume fraction in the slug for horizontal gas–liquid slug flow. *Int. J. Multiphase Flow* **4,** 33–39.

HERRINGE, R. A. & DAVIS, M. R. 1976 Structural development of gas–liquid mixture flows. *J. Fluid Mech.* **73,** 97–123.

HEYWOOD, N. I. & RICHARDSON, J. F. 1979 Slug flow of air–water mixtures in a horizontal pipe: determination of liquid holdup by gamma-ray absorption. *Chem. Engng Sci.* **34,** 17–30.

VAN HOUT, R. 1991 Experimental study of hydrodynamic parameters in vertical upward slug flow. M.Sc. Thesis, Tel-Aviv Univ.

MAO, Z.-S. & DUKLER, A. E. 1989 An experimental study of gas–liquid slug flow. *Expts Fluids* **8,** 169–182.

MAO, Z.-S. & DUKLER, A. E. 1991 The motion of Taylor bubbles in vertical tubes. II: Experimental data and simulations for laminar and turbulent flow. *Chem. Engng Sci.* **46,** 2055–2064.

MOISSIS, R. & GRIFFITH, P. 1962 Entrance effects in a two-phase slug flow. *J. Heat Transfer* **84,** 29–39.

NICHOLSON, M. K., AZIZ, K. & GREGORY, G. A. 1978 Intermittent two phase flow in horizontal pipes: predictive models. *Can. J. Chem. Engng* **56,** 653–663.

SCHMIDT, Z. 1977 Experimental study of two-phase slug flow in a pipeline–riser pipe system. Ph.D. Thesis, Univ. of Tulsa, OK.

SERIZAWA, A., KATAOKA, I. & MICHIYOSHI, I. 1975 Turbulence structure of air–water bubbly flow. II. Local properties. *Int. J. Multiphase Flow* **2,** 235–246.

SHEMER, L. & BARNEA, D. 1987 Visualization of the instantaneous velocity profiles in gas–liquid slug flow. *PhysicoChem. Hydrodynam.* **8,** 243–253.

TAITEL, Y., BARNEA, D. & DUKLER, A. E. 1980 Modeling flow pattern transition for steady upward gas–liquid flow in vertical tubes. *AIChE Jl* **26,** 345–354.

TAITEL, Y. & BARNEA, D. 1990 Two-phase slug flow. *Adv. Heat Transfer* **20,** 83–132.

VAN ATTA, C. W. 1974 Sampling techniques in turbulence measurements. *A. Rev. Fluid Mech.* **6,** 75–91.

ZUN, I. 1988 Transition from wall void peaking to core void peaking in turbulent bubbly flow. In *Transient Phenomena in Multiphase Flow; ICHMT International Seminar* (edited by AFGAN, N. H.), pp. 225–245. Hemisphere, Washington, D.C.

ZUN, I. & MOZE, S. 1990 Void fraction profile evolution in bubbly flow. Presented at the *25th Eur. Two-phase Flow Gp Mtg*, Varese, paper B2.